Fusing sEMG and EEG to Increase the Robustness of Hand Motion Recognition Using Functional Connectivity and GCN

Shiqi Yang, Min Li, *Member, IEEE,* Jiale Wang

***Abstract*—Surface electromyogram (sEMG) is widely used in active rehabilitation control for stroke patients. However, the accuracy of movement recognition using sEMG signals is affected by abnormal states such as muscular fatigue and muscle weakness. In this paper, a multi-modal fusion strategy of electroencephalogram (EEG) and sEMG is proposed to improve the accuracy and robustness of hand motion recognition. It is an end-to-end approach based on graph theory, in which the temporal signals of EEG and sEMG are considered as the features of nodes, and the functional connectivity is considered as the weights of edges. Four topologies, namely 2EnMe, 2EwMe, 5EnMe, and 5EwMe, are proposed, and two standardization methods are tested for each topology. Then, three functional connectivity methods are investigated, namely Pearson coefficient, mutual information, and coherence. Ten rounds of five-fold cross-validation show that GCN-2EnMe with the Pearson coefficient and min-max standardization is the best fusion model. At the fatigue levels of 0% and 30%, the achieved average accuracies are respectively 93.86% and 91.23%, which are significantly higher than those when using a parallel fusion method and a single-modality model. Moreover, the accuracy decrease ratio (ADR) of GCN-2EnMe is 2.80%, which is considerably better than that of a convolutional neural network (CNN) with parallel fusion (7.87%) and a CNN with single-modality sEMG (11.15%). The results show that the proposed novel EEG and sEMG fusion method has the potential to improve the accuracy and reliability of active control for stroke rehabilitation.**

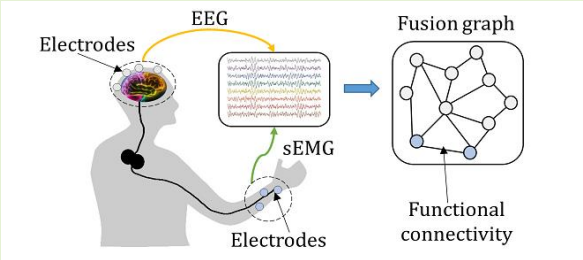

***Index Terms*—Multimodal fusion, EEG, EMG, muscular fatigue, graph theory**

I. Introduction

FOR stroke patients, active rehabilitation training with the voluntary participation of patients can improve the rehabilitation effect [1], [2]. Therefore, human-machine interfaces (HMIs) are widely used for the active control of rehabilitation devices, in which the electroencephalogram (EEG) and surface electromyogram (sEMG) are commonly used for the manifestation of motion intention [3]–[6]. However, the single-modality manipulation of EEG or sEMG cannot sufficiently satisfy the requirements of active control. For instance, the sEMG signals of stroke patients could be too weak to manifest their motion intention [7], and muscular fatigue will deteriorate sEMG signals [9], [8]. In contrast to sEMG signals, EEG signals have a lower amplitude and a larger amount of noise, which makes them less accurate and unreliable [10], [11]. Therefore, the use of single-modality decoding via EEG or sEMG for motion intention is not the optimal solution.

Multi-modal fusion can capture the complementary information of different modalities, thus improving the recognition accuracy and prediction robustness [12]. Many scholars have proposed approaches for the fusion of EEG and sEMG [5], [9]–[11], [13]. Nevertheless, most of the existing fusion methods are model-agnostic approaches [12] that mainly rely on manually-selected features. Leeb et al. [9] extracted the power spectral density (PSD) features of EEG signals and the threshold features of motions to train two Gaussian classifiers, respectively. The EEG and sEMG classification results were then fused by a Naïve Bayesian method to predict the final result. The accuracies of EEG and sEMG were respectively 73% and 83%, and the accuracy of the fusion of the two modalities reached 93%. Al-Quraishi et al. [5] employed discriminant correlation analysis (DCA) to fuse 21 EEG channels with sEMG signals, and used the linear discriminant analysis (LDA), k-nearest neighbors (k-NN), Naïve Bayesian, random forest, and decision tree models to classify four classes of ankle motion. Li et al. [10] extracted the temporal features of EEG and sEMG signals and used parallel concatenation to fuse the features, after which five classes of hand motions of amputees were classified by LDA. Chowdhury et al. [11] used the correlation between band-limited power time-courses (CBPT) as the fused features of EEG and sEMG to classify hand grasp motion, and achieved an accuracy of $84.53 \pm 4.58\%$ for the group of disabled patients. However, these existing methods are characterized by several defects. First, the features are extracted by human-designed algorithms, which may lose

Manuscript received August 23, 2022; Revised October 28, 2022; Accepted x x, 2022. This work was supported in part by the National Natural Science Foundation of China (Grant No. 51975451). S. Yang and M. Li are co-first authors. (Corresponding author: Min Li; E-mail: min.li@mail.xjtu.edu.cn).

S. Yang, M. Li, and J. Wang are with the Department of Mechanical Engineering, Xi'an Jiaotong University, Xi'an 710049, China.

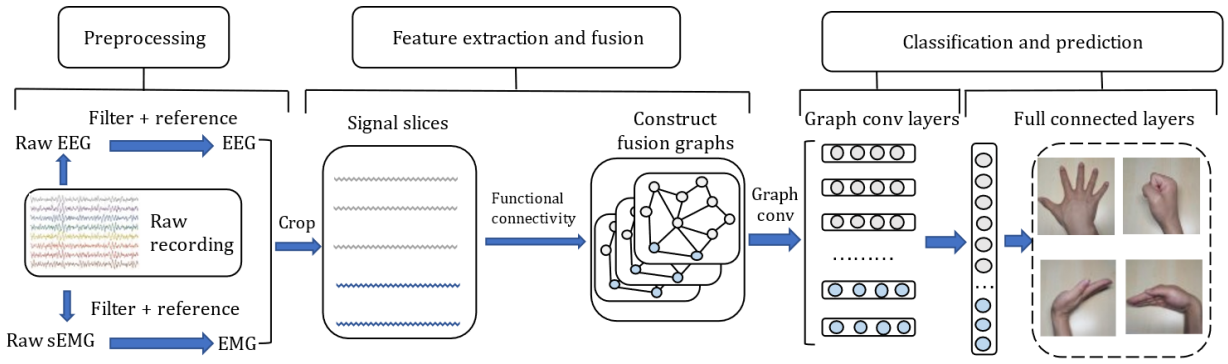

Fig. 1. The overview of the GCN-based Fusion Strategy for EEG and sEMG (GFSEs).

the intrinsic information of the raw data [14]. Second, the fusion and prediction processes are separated, thus it hinders the model from optimizing different parts of itself [15]. Third, there are relationships between the spatial distribution and functional couplings of the EEG and EEG channels and the EEG and sEMG channels [16], [17]. While the conventional fusion methods only fuse the features at the numerical level, which ignores the real-world connections between the different channels.

Neural network is a model-based fusion approach that has shown promising performance in many assignments [12], and it can automatically complete feature extraction and fusion, as well as end-to-end prediction [15]. It solves the first two problems mentioned above, but still fails to manifest the couplings and spatial distribution of sEMG and EEG. For instance, as one of the most famous deep learning methods, the convolutional neural network (CNN) has shown excellent classification ability in many assignments [18], [19], but it can only deal with regularized input such as pictures or videos [16]. In essence, due to the spatial distribution of EEG and sEMG electrodes and the functional couplings between them [13], graph is a more appropriate description.

Graph theory is more advantageous in dealing with signals from the discrete spatial domain [20]. As an extension of CNN, graph convolutional network (GCN) has shown brilliant performance in the feature extraction and classification of EEG signals. For instance, Song et al. [16] built the Dynamical Graph Convolutional Neural Network (DGCNN), which takes the PSDs of different EEG channels as the input to classify six categories of emotions. Li et al. [21] proposed the Graph-based Convolutional Recurrent Attention Model (GCRAM), which represents the spatial characteristics by graph embedding and uses a convolutional recurrent attention network to extract features and fulfill classification. They also investigated the influence of three different connections on accuracy. Although GCN is successful in dealing with EEG-related assignments, to the best of the authors' knowledge, it has not yet been employed in building a model-based fusion approach for EEG and sEMG.

In this work, the GCN-based Fusion Strategy for EEG and sEMG (GFSEs) is constructed. It aims at providing a more accurate and robust solution for the recognition of hand motion intention under muscle fatigue situation. That method has the potential to improve the accuracy and reliability of active control for stroke rehabilitation. The three steps of feature extraction, feature fusion, and classification are connected and coherent, which enables the model to learn from each step and realize end-to-end prediction. There are two reasons of building fusion model based on GCN. First, GCN is one of the powerful and widely used models in deep learning [22], and it can process non-Euclidean structure data and complete computation fast [23]. Second, compared with other graph neural networks (GNNs) that focus on the features of each node, GCN manifests the global information of the whole graph [24]. This matches the requirement of using multiple electrodes to represent user's intention.

The construction of an sEMG and EEG fusion graph faces numerous challenges. First, unlike EEG graphs, in which the distribution of the EEG electrodes is definite according to brain regions [15], [16], the electrodes of muscles and brain neurons do not share a definite spatial distribution. Therefore, the proper topological structure of the fusion graph should be studied. Second, the edge weights of the fusion graph are crucial for graph convolution. Thus, the appropriate connection should be investigated. Third, the amplitude of EEG signals is much weaker than that of sEMG signals [25]; if the two signals are directly input into the graph, the EEG information may be neglected. Thus, a suitable standardization method should be investigated to make full use of the intrinsic information of both types of signals.

In this paper, three key problems are investigated, including the topologies of the fusion graph, the functional connectivity between nodes, and the proper standardization approach for the fused data. In the experiments, all the models are tested by sEMG at a 0%-30% "fatigue" level via 10 rounds of five-fold cross-validation. Four different fusion graphs with two different standardization methods are tested, and the effects of several functional connectivity approaches are then investigated. Finally, the best model is compared with the other models using parallel fusion approach and models of single-modality data.

The arrangement of the remainder of this paper is as follows. Section II introduces the methodology of the fusion model. Section III describes the data acquisition protocol and the experiments in terms of the accuracy of different models. Section IV discusses the phenomena observed in this work, and Section V provides the final conclusion.

II. Methodology

A. Overview of the Multi-Modal Fusion Method

The overview of the proposed GFSEs is shown in Fig. 1. The

This article has been accepted for publication in IEEE Sensors Journal. This is the author's version which has not been fully edited and content may change prior to final publication. Citation information: DOI 10.1109/JSEN.2022.3221417

whole process consists of three procedures: preprocessing and standardization, feature extraction and fusion, and classification and prediction. It is an end-to-end approach in which the raw EEG and sEMG signals are separately pre-processed and then cropped along the temporal sequence. After pre-processing, the data is cropped into segment and standardized within the segment. Then functional connectivity values of each two channels are computed and assigned to the corresponding edges of the graph. Finally, the data of each channel is input into the matching nodes to complete the construction of one fusion graph. In essence, each graph represents the state of motion intention during a specific period, and its features are extracted and fused by the GCN. Then, a fully connected (FC) network completes the prediction procedure.

B. Recording and Pre-processing of EEG and sEMG Data

In this study, 12 channels of EEG signals and 4 channels of sEMG signals were simultaneously recorded by SynAmps2 (Neuroscan, USA) at a rate of $f_s = 500$ Hz. All the EEG electrodes were positioned according to the international 10-10 system using Ag/AgCl electrodes. The involved EEG electrodes were FZ, FC1, FCZ, FC2, C3, C1, CZ, C2, C4, CP1, CPZ, CP2, PZ, M1, and M2. M1 and M2 were the reference electrodes. Moreover, the bi-polar sEMG electrodes on the right arm of the subjects were positioned according to the Surface EMG for Non-Invasive Muscle Evaluation (SENIAM, seniam.org) criteria. The sEMG differential electrodes 1 to 4 were mounted on the extensor digitorum, extensor carpi radialis, superficial digital flexor, and flexor carpi ulnaris of all the subjects, respectively.

Let N_e and N_m represent the number of EEG and sEMG channels, respectively, and $N_a = N_m + N_e$ is the total number of electrodes. In each recording, the raw data were a two-dimensional (2D) matrix $\boldsymbol{X} \in \mathbb{R}^{N_a \times k}$. Each row represents the recording samples $\boldsymbol{R}_{i\,|i\in[1,N_a]} = \left[p_1^i, p_2^i, \ldots, p_K^i\right]$ from the i-th electrode, where $K = T \times f_s$, and T is the duration of the recording. Then, the EEG signals were bandpass-filtered between 1 and 70 Hz, and the EMG signals were filtered by a fourth-order Butterworth bandpass filter between 10 and 200 Hz.

It is difficult to quantify fatigue levels, and the subjective feelings of subjects are inaccurate. To assess the robustness of the fusion method, Leeb et al. [9] degraded the amplitude of sEMG signals to simulate muscular fatigue at different levels. In this study, a simulation method was employed to produce graded fatigue sEMG signals at fatigue levels of 0%-30%. As shown in Equation (1), They were simulated by degrading the amplitude of the sEMG signal and adding a proportional Gaussian noise to it. The percentage of Gaussian noise is defined according to the signal-to-noise ratio (SNR). The reasons of adding noise are: when fatigue increases, the variance of EMG's amplitude will increase, and its root mean square will rise[26]-[28]. Besides, reducing the amplitude simulates the exhausted situation of participant. For instance, a 10% fatigue sEMG signal is produced by adding a 10% Gaussian noise to the signal which has been 10% reduced (has 90% amplitude of the original signal).

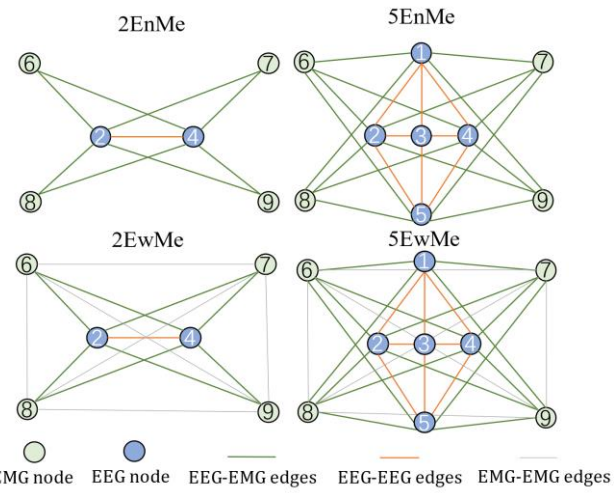

Fig. 2. The constructures of the four fusion graphs. From 1 to 9, the channels are FC, C3, CZ, C4, PZ, sEMG1, sEMG2, sEMG3, sEMG4.

$$\begin{cases} \varepsilon_{n\,|n\epsilon[0,0.1,0.2,0.3]} = \sqrt{\dfrac{P_N}{P_S}} \\ \boldsymbol{Rf}^i_{n\,|n\epsilon[0,0.1,0.2,0.3]} = \boldsymbol{R}_i \times (1-n) + \varepsilon_n \times \boldsymbol{Rn_i} \end{cases}, \quad (1)$$

where ε_n is the percentage of Gaussian noise, P_N and P_S are respectively the noise signal power of $\boldsymbol{R}_i$, $\boldsymbol{Rf}^i_n$ is the simulated fatigue signal from 0 to 30%, and $\boldsymbol{Rn_i}$ is a random vector that has the same size as $\boldsymbol{R}_i$ in a standard normal distribution.

C. Functional Connectivity of EEG and sEMG Signals

In this section, three approaches of functional connectivity are employed to represent the couplings of EEG with sEMG and EEG with EEG. Pearson coefficient, mutual information, and coherence are employed as the weights of edges, and they are computed by Equations (2), (3), and (4), respectively. For all of the equations, when applied in EEG-EEG channels they represent the synchronization of brain regions and the activity patterns of brain [30], [31]. When applied in EEG-sEMG channels, they describe the information transmission of the loop between cortex and muscle, thus manifest the causation of sEMG by EEG [33],[25].

$$r = \frac{\sum(x - m_x)(y - m_x)}{\sqrt{\sum(x - m_x)^2 \sum\left(y - m_y\right)^2}}, \quad (2)$$

where x and y are the two vectors used to compute the functional connectivity, r is the Pearson coefficient, and m_x and m_y are the mean values of the vectors, respectively.

$$C_{xy} = \frac{abs\left(P_{xy}\right)^2}{\left(P_{xx} \cdot P_{yy}\right)}, \quad (3)$$

where C_{xy} is the coherence of x and y, P_{xx} and P_{yy} are the PSDs of x and y, respectively, and P_{xy} is the cross-spectral density of x and y.

$$\begin{cases} I(x;y) = \sum_x \sum_y \rho(x,y) \log\left(\dfrac{\rho(x,y)}{\rho(x)\rho(y)}\right) \\ NorMI(x;y) = \dfrac{I(x;y)}{\sqrt{H(x)H(y)}} \end{cases}, \quad (4)$$

where $I(x;y)$ is the mutual information between x and y, and $\rho(x)$ and $\rho(y)$ are the probability density functions of x and y, respectively. The joint probability density is defined as $\rho(x,y)$, $H(x)$ and $H(y)$ are the Shannon entropies of x and y, respectively, and $NorMI(x;y)$ is the normalized mutual information.

For each edge, its functional connectivity is $W_i = F_{fc}(\boldsymbol{Rw}_m, \boldsymbol{Rw}_n)$, where $i \epsilon M_e$ is the index of the edges, $m, n \epsilon [1, N_a]$ are the indexes of the nodes, and F_{fc} is the connectivity computation method. According to previous studies [25] , [32], coherence within 10–15 Hz is set as the edge weight. Moreover, the weights of the Pearson coefficient and mutual information are normalized by min-max standardization. The performance of all the connectivity approaches was tested, as reported later.

D. Standardization and Topological Structure of the Fusion Graph

An undirected graph $G = (\boldsymbol{X_w}, \boldsymbol{E}, \boldsymbol{A})$ is constructed for each window of the signals. In each graph, the temporal signal sequence $\boldsymbol{Rf}_n^i$ is cropped into slices $\boldsymbol{Rw}_{i\,|i\in[1,N_a]} = [p_1^i, p_2^i, \ldots, p_{Kw}^i]$ via a sliding window to manifest local features, where $Kw = Tw \times f_s$, and Tw is the length of the sliding window. Moreover, $\boldsymbol{Rw}_i$ are the features of the i-th node of graph G, and $\boldsymbol{X_w}$ is the feature matrix of graph G. Finally, A $\in \mathbb{R}^{N_a \times N_a}$ is a binary or weighted adjacency matrix describing the connections between the nodes, $\boldsymbol{E}_{i|i\epsilon M_e}$ represents the edges between the nodes, and M_e is the total number of the edges.

As shown in Fig. 2, four topological structures of the fusion graph are proposed: 2 EEG with no sEMG-sEMG edges (2EnMe), 5 EEG with no sEMG-sEMG edges (5EnMe), 2 EEG with sEMG-sEMG edges (2EwMe), and 5 EEG with sEMG-sEMG edges (5EwMe). In EEG map, C3, C4 and CZ are electrodes located in brain's sensory and motor region, and the movement of right hand has significant effects on the potential of C3 and C4 [29]. Moreover, refer to the design in [11], PZ and FCZ are also added into the graph to give a comprehensive description of brain activity. All the EEG nodes are placed by spatial position and connected to neighboring nodes, and all the sEMG nodes are connected to each of the EEG nodes through functional connectivity. EMG-EMG connection of each node is also constructed to test whether it has a positive effect or not.

For each graph, the feature matrix $\boldsymbol{X_w}$ is standardized by Z-score standardization (5) and min-max standardization (6), respectively. Additionally, the edges of the graphs are weighted by the corresponding values of functional connectivity. The datasets of fusion graph $Gd^i_{n=[0,0.1,0.2,0.3]}$ were constructed, and their performance was experimentally investigated, as described later.

$$\frac{p_i - \mu}{\sigma}, \tag{5}$$

$$\frac{p_i - p_{min}}{p_{max} - p_{min}}, \tag{6}$$

where p_i is the signal sample in a column of $\boldsymbol{X_w}$, p_{min} is the minimum value of the column, p_{max} is the maximum value of the column, μ is the mean value of the column, and σ is the standard deviation of the column.

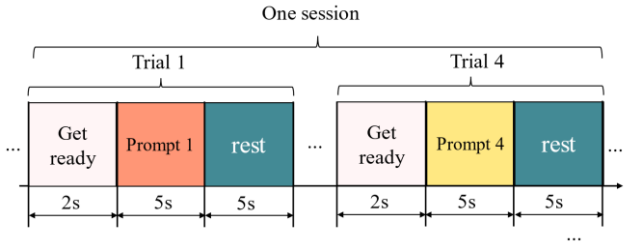

Fig. 3. The experiment protocol of acquisition of EEG and sEMG signal. A session contains four trials.

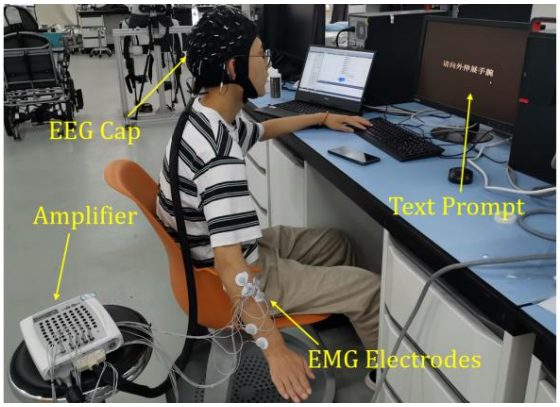

Fig. 4. The setting of the acquisition system.

TABLE I
THE PARAMETERS OF THE FUSION AND PREDICTION MODEL

Layer	Input size	output size	Operation
GCN layer 1	(N_a, kw)	$(N_a, 512)$	$Relu(x)$
GCN layer 2	$(N_a, 512)$	$(N_a, 256)$	$BN(Relu(x))$
Flatten layer	$(N_a, 256)$	$(1, N_a \times 256)$	None
FC layer1	$(1, N_a \times 256)$	(1,1024)	$BN(Relu(x))$
FC layer2	(1,1024)	(1,512)	$BN(Relu(x))$
FC layer3	(1,512)	$(1, class)$	$softmax(Relu(x))$

E. Graph Convolution and Model Training

In this work, GCN is employed to learn the fusion graph representation, and the fusion features are sent to FC layers to output the final prediction. The specific operation of graph convolution was described in a previous work [34], and the basic format of graph convolution is given by Equation (7):

$$H^{l+1} = \sigma(\tilde{D}^{-\frac{1}{2}} \cdot (\tilde{D} - \bar{A}) \cdot \tilde{D}^{-\frac{1}{2}} \cdot H^l \cdot W^l), \tag{7}$$

where $H^l \in \mathbb{R}^{N_a \times \mathrm{kl}}{}_{|l\in[1,tmax]}$ is the l-th feature matrix, $W^l \in \mathbb{R}^{\mathrm{kl} \times \mathrm{n}}{}_{|l\in[1,tmax]}$ is the l-th weight matrix, $tmax$ is the maximum training time, and kl is the length of the features of each node in the l-th iteration. Moreover, $\tilde{D} \in \mathbb{R}^{N_a \times N_a}$ is the degree matrix of the graph, $\bar{A} \in \mathbb{R}^{N_a \times N_a} = \mathrm{A} + \mathrm{I}$, and σ is the activation function.

The GCN could be perceived as a form of Laplacian smoothing, the deeper layer would cause over-smoothing [35], so the layers should not be too deep. According to the previous studies, the GCN layers are often set as two [16], [36]; thus, two GCN layers are used in the model. Three FC layers are added after the GCN layers to fully classify the features. As reported in Table I, the detailed parameters of the GCN and FC layers are set by experience and tests, and x is the tensor in the forward process. The last GCN layer represents the graph G by a feature

TABLE II
COMPARISON ON THE ACCURACY OF THE DIFFERENT TOPOLOGIES AND STANDARDIZATION METHODS

Subject	Fatigue level	Accuracy of Min-max standardization dataset %				Accuracy of Z-score standardization dataset %			
		2EnMe	2EwMe	5EnMe	5EwMe	2EnMe	2EwMe	5EnMe	5EwMe
S1	0%	**96.80±0.23**	94.62±0.29	96.34±0.33	94.12±0.36	95.03±0.53	92.17±0.79	91.72±0.37	81.70±0.65
S2	0%	**87.26±0.38**	87.10±0.11	84.79±0.38	82.10±0.26	85.59±0.99	86.31±0.31	83.87±0.58	74.02±0.80
S3	0%	**98.14±0.11**	97.57±0.36	97.69±0.20	97.08±0.28	97.12±0.40	95.72±0.26	95.35±0.26	91.93±0.40
S4	0%	**91.31±0.27**	91.00±0.32	89.78±0.17	89.94±0.92	89.84±0.05	89.77±1.14	82.93±0.98	77.26±1.03
S5	0%	**98.66±0.15**	98.51±0.21	98.22±0.21	97.39±0.36	97.84±0.33	97.44±0.18	92.48±0.60	84.04±0.52
S6	0%	**85.50±0.52**	81.85±0.58	83.56±0.66	81.87±0.53	83.04±0.77	78.62±0.77	78.43±0.69	69.56±1.11
S7	0%	**98.24±0.21**	97.84±0.11	96.84±0.32	97.23±0.21	97.72±0.24	96.36±0.25	93.94±0.41	91.14±0.54
S8	0%	**95.00±0.78**	94.39±0.21	94.00±0.46	93.58±0.49	91.70±0.52	82.52±0.13	81.82±0.68	61.95±1.21
Average of all subjects	0%	**93.86±5.22**	92.86±5.88	92.65±5.88	91.66±6.47	92.24±5.71	89.86±6.89	87.57±6.48	78.95±10.38
	10%	**93.21±5.38**	92.45±6.00	92.22±6.08	91.15±6.42	91.23±6.28	89.03±6.66	86.87±6.43	77.34±10.08
	30%	**91.23±5.11**	89.87±6.06	89.66±6.35	88.04±6.51	86.66±7.13	81.71±7.47	80.02±7.17	65.56±8.93

matrix $P \in \mathbb{R}^{N_a \times kx}$, where kx is the number of features of the last GCN layer. Then, P is flattened and directly input into the FC layers, instead of being pooled. For each layer, $ReLU$ is the activation function, and batch normalization (BN) is used in the second GCN layer and every FC layer.

For all the experiments, the dataset Gd_n^i was validated via five-fold cross-validation by fatigue level. Before training, all the layers were initialized by Xavier. In each fold, the ratio of the training and testing datasets was 8:2, the number of training epochs was 40, and the training batch size was set as 32. For all the models, cross entropy was set as the loss function, and the learning rate of Adam optimizer was set as 0.0001.

III. EXPERIMENT AND RESULTS

A. Acquisition Experiments of EEG and sEMG Signals

Five male and three female subjects were recruited to collect their EEG and sEMG signals. They were all healthy postgraduate students with an average age of 23.8. Four motion classes were involved in the protocol, including wrist flexion (WF), wrist extension (WE), fist grip (FG), and five fingers open (FFO). During the experiments, each subject sat at a comfortable chair in a quiet room, and a computer screen was placed about 40 cm from the subject at a stable table. The recording system was initiated according to the criteria defined in Section II.B, and the EEG and sEMG signals were simultaneously documented. This study was reviewed and approved by the Institutional Review Board of Xi'an Jiaotong University (Approval No. 2019-584).

The acquisition protocol is shown in Fig. 3. For each subject, the experiment consisted of 40 repeated sessions, each session contained four trials, and one movement was presented in each trial. At the beginning of the experiment, the subject was instructed about the protocol and asked not to move their body during the recording. Before each trial, a sign of "ready to start" appeared on the screen and lasted for 1 second, and then a short text denoting "wrist flexion," "wrist extension," "fist grip," or "fingers open" was displayed on the screen in random order. Each prompt lasted for 5 seconds, and the subject maintained the motion for the duration of the prompt. Between every two trials, there was a 5-second rest. After 10 consecutive sessions, the subjects could rest until they were not fatigued. In total, 40 sessions × 4 movements × 5 seconds = 1760 seconds of activation data was acquired for each subject. Considering the signals from 1s to 4s after the prompt as the valid data, a window with a length of 200 recording points and a step of 200 was employed to crop the data. Then dataset Gd_n^i was constructed. Under each fatigue level, 1,120 graph samples are included.

TABLE III
P-VALUES BY K-W TEST AND M-W TEST FOR DIFFERENT TOPOLOGIES

Subject	P-values of K-W test	P-values of Mann-Whitney test		
		2EnMe with 2EwMe	2EnMe with 5EnMe	2EnMe with 5EwMe
S1	3.91E-05	1.83E-04	1.83E-04	1.83E-04
S2	6.67E-01	3.45E-01	9.10E-01	1.00E+00
S3	1.33E-05	1.83E-04	1.83E-04	1.83E-04
S4	2.55E-05	1.83E-04	1.83E-04	1.83E-04
S5	9.52E-01	9.70E-01	7.91E-01	8.50E-01
S6	6.66E-05	1.83E-04	1.83E-04	1.83E-04
S7	8.03E-02	6.23E-01	2.41E-01	1.73E-02
S8	1.42E-04	7.69E-04	1.83E-04	2.46E-04

TABLE IV
COMPARISON ON THE ROBUSTNESS OF THE DIFFERENT TOPOLOGIES

Topology	Accuracy decreasing ratio (ADR)	
	Min-max standardization	Z-score standardization
2EnMe	2.80	6.12
2EwMe	3.23	9.11
5EnMe	3.26	8.66
5EwMe	3.97	16.94

B. Experiments on the Accuracy and Robustness of the Different Topologies and Standardization Methods

In this section, the Pearson coefficient was assigned as the weight values for all the edges of the eight graph datasets Gd_n^i. Then, they were tested via 10 rounds of five-fold cross-validation. The experimental results are reported in Table II. For each subject, the mean accuracies and standard deviations are listed by fatigue level. The bold numbers indicate the highest accuracy in each row.

The results reveal four conclusions. First, the topology 2EnMe obtained the highest accuracy among all the topological structures under three different fatigue levels. The highest accuracy was 98.66%, which was achieved by subject 5. Second, when the topology was the same, the group of using min-max standardization had higher accuracies than those of using Z-score standardization. Third, when the basic topology was the same, adding EMG-EMG connections would reduce the accuracy. For example, in min-max group, the average accuracy of 2EnMe was 93.86%, but that of 2EwMe was 92.86%. Fourth, when other parameters were the same, the graphs using 2 EEG nodes obtained better accuracies than those with 5 EEG nodes.

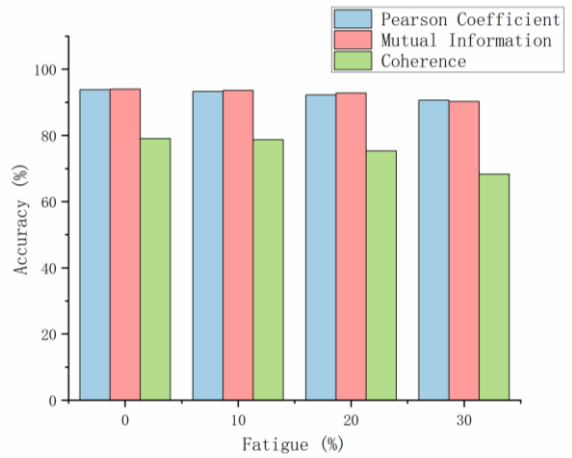

Fig. 5. The average accuracies of graphs using three different functional connectivity methods.

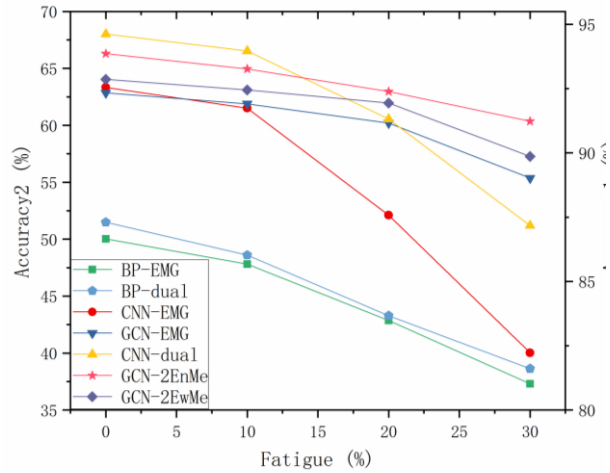

Fig. 6. The average accuracies of different fusion methods. BP-EMG and BP-dual correspond to the axis of Accuracy2, and the other groups correspond to the axis of Accuracy1.

TABLE V
P-VALUES BY K-W TEST AND M-W TEST FOR DIFFERENT MODELS

Subject	P-values of K-W test	P-values of Mann-Whitney test		
		2EnMe with CNN-dual	2EnMe with GCN-EMG	2EnMe with CNN-EMG
S1	5.63E-08	1.83E-04	1.83E-04	1.83E-04
S2	5.63E-08	1.83E-04	1.83E-04	1.83E-04
S3	5.63E-08	1.83E-04	1.83E-04	1.83E-04
S4	5.63E-08	1.83E-04	1.83E-04	1.83E-04
S5	2.84E-07	1.83E-04	2.73E-01	1.83E-04
S6	2.37E-07	1.04E-01	1.83E-04	1.83E-04
S7	6.48E-08	1.83E-04	3.30E-04	1.83E-04
S8	1.91E-07	1.83E-04	1.83E-04	1.83E-04

For instance, the average accuracy of 2EnMe group at three fatigue levels was 92.77%, and that of 5EnMe group was 91.73%.

To investigate the significance of the difference between the accuracies of various topologies, the Shapiro-Wilk test was first used to test whether the accuracies conformed to normal distribution. The result reveals that the distribution of accuracies was not a normal distribution, so the Kruskal-Wallis test was employed for the accuracies of 2EnMe, 2EwMe, 5EnMe, and 5EwMe under min-max standardization to test the significance of the overall difference. Then, the Mann-Whitney test was completed for the accuracies of 2EnMe and those of the other three topologies. As shown in Table III, the *P*-values are listed by subject. A *P*-value less than 0.05 indicates a significant difference. Except for subjects 2, 5, and 7, the topologies were found to have significant effects on the performance of accuracies. Furthermore, the performance of 2EnMe was considerably better than those of the other topologies.

In Table IV, the average accuracy decrease ratios (ADRs) of the four topologies under max-min standardization are demonstrated to show the robustness of these models. ADR is defined as $(AC_{0.3} - AC_0)/AC_0$, where AC_0 is the accuracy of the original data $Gd^i_{n=0}$, and $AC_{0.3}$ is the accuracy of the 30% fatigue data $Gd^i_{n=0.3}$. The Kruskal-Wallis test was conducted to investigate the significance of the differences between the ADRs of 2EnMe, 2EwMe, 5EnMe, and 5EwMe. The *P*-values of all subjects were found to be greater than 0.05, so it is assumed that the robustness of the four topologies was not considerably different. In summation, the topology of the graph was found to have a significant effect on the accuracy of recognition, while it does not affect the robustness of the fusion model.

C. Experiments on the Accuracy and Robustness of Different Functional Connectivity

In this section, the datasets Gd^i_n were copied to two groups, namely the mutual information group and coherence group. In each group, the values of the two functional connectivity approaches were employed as the weights of edges for 2EnMe to build fusion graphs. Then, 10 rounds of five-fold cross-validation were completed for all the fusion graphs. The accuracies and robustness of the graphs achieved using these two connectivity methods were compared with those achieved using Pearson coefficient.

The average accuracies of the four fatigue levels of all the subjects are illustrated in Fig. 5. Among the three functional connectivity approaches, the group using Pearson coefficient achieved the highest accuracy and lowest ADR (4.4%). The graphs weighted by mutual information achieved a performance slightly lower than those for which Pearson coefficient was used. The coherence of the alpha band achieved the lowest accuracy, which was 75.4% for non-fatigue data, and its ADR was the highest (14.1%). Therefore, from the perspective of both accuracy and robustness, Pearson coefficient is the best functional connection for this fusion graph.

D. Comparison of the Accuracy and Robustness of Different Fusion Models

To validate the effectiveness of the multi-modal fusion approach proposed in this paper, the accuracy and robustness of the fusion graph were contrasted to those of other methods, including those obtained by only using sEMG signals and using the parallel fusion of sEMG and EEG signals. The contrasting classifiers were the CNN and back-propagation (BP) network. The three single-modality groups were CNN-EMG, GCN-EMG, and BP-EMG, which respectively employed the CNN, GCN, and BP to classify the EMG signals. It should be noted that all the EMG nodes in the GCN-EMG group were connected to each other by values of the Pearson coefficient. In contrast, the three

TABLE VI
COMPARISON WITH THE OTHER FUSION MODELS

Research	Window size	Category	Accuracy of raw data	Accuracy of fatigue data	Fusion methods	Classifier
[5]	500 samples (non-overlap)	2 movements	Average at 96.6±4.48% on all subjects	95.45±5.33% for the acquired fatigue data	DCA fusion	LDA
[10]	150 samples (33% overlap)	4 movements	80.7-94.2% on single subject	/	Linear combination	LDA
[38]	/	2 movements	Average of 86.81 ± 3.98% on all subjects	Falls to 77.48 ± 8.73%	AND, Weighted Average	SVM
GFSEs	200 samples (non-overlap)	4 movements	Average at 93.86±5.22% on all subjects	Remain 91.23±5.11% when fatigue level reaches 30%	Graph theory	GNN

dual-modality groups were CNN-dual, GCN-dual, and BP-dual, among which GCN-dual used 2EnMe and 2EwMe to fuse the EEG and sEMG signals, while the other two employed the parallel fusion method. To reduce the number of variables, the CNN classifier used in this experiment had two convolutional layers and three FC layers. Its FC layers had identical parameters to those of the GCN model. The BP network consisted of three FC layers, and its parameters were the same as those in the CNN model.

The average accuracies of different models for all subjects are shown in Fig. 6. All the dual-modality methods achieved higher accuracies than the corresponding single-modality methods when dealing with data at the same fatigue level. The CNN-dual model achieved the highest accuracy improvement as compared to CNN-EMG at the 30% fatigue level, which was 4.95%. However, the improvement of the BP network was not significant, and its average accuracies were the lowest. Compared to GCN-EMG and CNN-EMG, the fusion graph 2EnMe achieved average accuracy improvements of the four fatigue levels of 1.45% and 4.16%, respectively. Nevertheless, the highest accuracy was achieved by the CNN-dual model at the fatigue level of 0%, and the robustness of 2EnMe was much better than that of CNN-dual. Moreover, the ADRs for CNN-dual and CNN-EMG were 7.87% and 11.15%, respectively, while that of 2EnMe was 2.80%. When the fatigue level exceeded 20%, the graph-based models achieved higher accuracies.

To investigate the significance, the accuracies of CCN-2EnMe, CNN-dual, CCN-EMG, and GCN-EMG at various fatigue levels were tested by the Kruskal-Wallis test. The P-values are shown in Table V; all of them are less than 0.05, which means that the graph fusion method exhibited a significant difference in accuracy as compared to the parallel fusion and single-modality methods. Then Mann-Whitney test was conducted to demonstrate the significance between GCN-2EnMe and other models. Except for the GCN-EMG model for subject 5 and the CNN-dual model for subject 6, the accuracies of GCN-2EnMe exhibited a significant difference from those of the other models for all the other subjects. This experiment proves two results. First, the fusion of EEG and sEMG can improve the recognition accuracy of hand motions. Second, compared with parallel fusion, the graph fusion method can achieve better robustness when dealing with fatigue data.

IV. DISCUSSION

A. Comparison with the Contemporary Fusion Methods

The proposed GFSEs method is also compared with the other contemporary fusion methods for EEG and sEMG signals introduced in [5], [10], [38]. As shown in Table VI, the average accuracy of GFSEs is higher than [38] and [10], but slightly less than research [5]. It may due to the number of category and

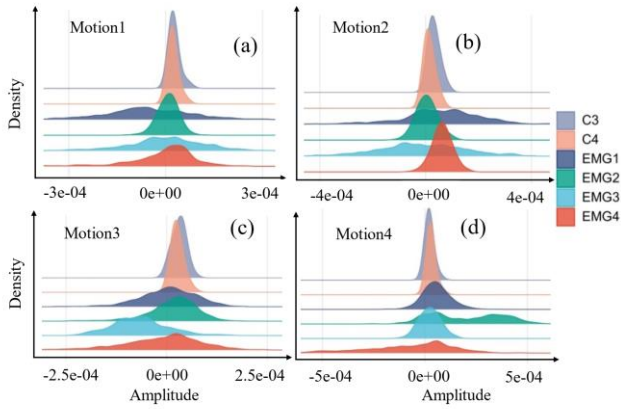

Fig. 7. The density distribution of different motions: (a) motion 1, (b) motion 2, (c) motion 3, and (d) motion 4.

difference between muscles that used in recognition. Our method uses a non-overlap and much shorter window to crop the data. While generally, larger window size and more overlapping contributes to higher accuracy but longer time expenditure. That indicates the proposed method may have a greater ability in fusion and extraction of features.

The core advantage of GFSEs is it can maintain a higher accuracy during the increasing of muscle fatigue. When fatigue level increases from 0% to 30%, the accuracy just slightly drop to 91.23% from 93.89%. In research [9], the accuracy of fusion method falls to 73% when EMG decreases to 10% of the original amplitude. In reference [5], the accuracy of fusing acquired fatigue sEMG is not significantly less than that of non-fatigue sEMG. In terms of fatigue data, the average accuracy falls to 77.48% from 86.81% in reference [38]. Compared with the existing research, GFSEs has a better robustness in handling increasing fatigue or abnormal sEMG data. Here our proposed method is only compared with other fusion methods applied for EEG and sEMG signals. Other methods used for fusing EMG with inertial motor unit data or fusing EEG with fMRI signals can be explored in the future.

The central contribution of this method is to construct a model represents the real state of human's motion intention through graph theory. Functional connectivity manifests the synchronization between brain nerves and the neural path of nerves to muscles. In this paper, GCN is employed to process the graph data. However, the other GNNs are worth to be tested in the future, such as Graph Attention Network (GAT) etc.

B. Standardization Methods for the EEG and sEMG Signals in the Fusion Graph

In the proposed GFSEs, the EEG and sEMG signals are directly input as the node features of the fusion graph. Because the original signals are only filtered, rather than

This article has been accepted for publication in IEEE Sensors Journal. This is the author's version which has not been fully edited and
content may change prior to final publication. Citation information: DOI 10.1109/JSEN.2022.3221417

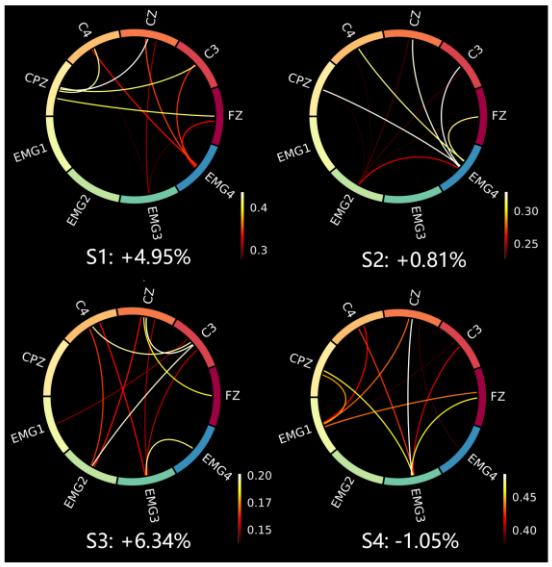

Fig. 8. The average intensity of PLI connectivity of all motions of all the subjects. The percentage after the subject number is the average improvement in accuracy of three fatigue levels.

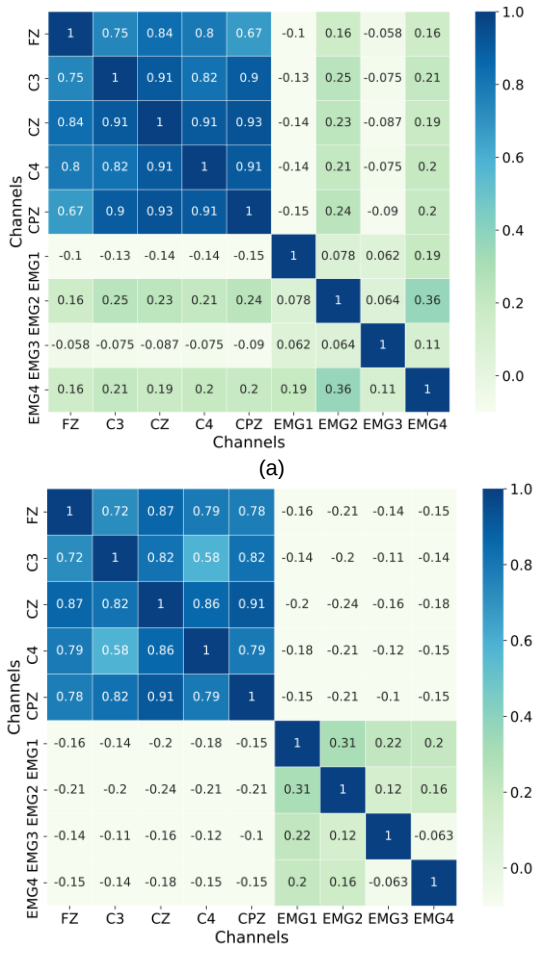

Fig. 9. The Pearson coefficient matrix of two subjects: (a) subject 5 and (b) subject 4.

feature-extracted, the standardization of sEMG and EEG plays a vital role in the pre-processing. The results of the experiments show that min-max standardization achieved better performance in almost all the subjects in terms of accuracy and robustness. To explore the possible reason for this phenomenon, the data of one session of subject 1 was analyzed as an instance.

The density distributions of C3, C4, and EMG1 to EMG4 were respectively drawn for the four motions. As shown in Fig. 7, when performing different motions, the density distributions of the EEG and sEMG signals varied significantly. For instance, for motion 1, the amplitude distribution of EMG1 was wider and more skewed to the left. For action 4, the amplitude distribution of EMG1 was narrower, and the distribution of EMG4 was wider and shifted toward the left. In all the motions, the distribution of the EEG signals was concentrated around 0. Therefore, the distributions of the signals are also a characteristic of different actions. It is possible that Z-score standardization changed the distributions; thus, it reduced the number of features that could be identified, and the classification accuracy was less than that when using min-max standardization.

Batch normalization is used in various neural networks and has achieved great performance in promoting both the accuracy and training speed [19], [22]. Although the function of Z-score standardization is also to normalize the data into the normal distribution, it is not suitable for the fusion graphs. As explained previously, the application of Z-score standardization to the whole dataset may eliminate the distribution characteristics. Thus, Z-score standardization can be applied within the batch, which may reserve the distribution characteristics and attain better performance. However, more standardization methods should be investigated in the future to find the optimal method for EEG and sEMG signals.

C. The Effect of Different Topologies on the Performance of the Fusion Graphs

In this study, four fusion graphs with specific topologies were constructed. These graphs can be categorized into two groups, namely those with and without EMG-EMG connections, e.g., 5EnMe and 5EwMe. According to experiment II.B, when the number of EEG channels was equal, the groups without EMG-EMG connections achieved higher accuracy than the groups with EMG-EMG connections. This may be because when the EMG noise gets stronger, the EMG-EMG connections amplify the effect of the abnormal signals.

Nevertheless, the addition of EEG signals can increase the recognition accuracy, but more EEG channels cannot necessarily contribute to higher accuracy. When the EMG-EMG connection was the same, the graphs with 2 EEG channels achieved higher accuracy than the graphs with 5 EEG channels. For example, 2EnMe performed better than 5EnMe, and the accuracy of 2EwMe was greater than that of 5EwMe. There may be two reasons for this phenomenon. The first is that the selected EEG channels were not matched with the sEMG electrodes, so it was necessary to optimize the selection of the EEG channel to find the optimal combination. The second is that the noise of the EEG signals was too strong, which was not helpful for representing the motion intention. It may be more effective to extract features of EEG signals and feed the extracted features into the nodes of the graph.

D. The Effect of Functional Connectivity on the Performance of the Fusion Graphs

Taking GCN-EMG as the baseline, the two models (GCN-2EwMe, GCN-2EnMe) with added EEG-EMG connections were found to have an increased average accuracy and robustness. Except for subject 4, the average accuracies of all the subjects increased when using GCN-2EnMe. While compared with CNN-EMG, among the eight subjects, the three subjects with the smallest improvement in average accuracy were S4, S2, and S8, which were -1.05%, 0.81%, and 4.78%, respectively.

To explore the reasons why the addition of EEG signals can improve the recognition accuracy, and the reasons for the differences in the accuracy improvement of different subjects, the Phase Lag Index (PLI) [37] was introduced as the indicator of the functional connectivity for all the channels. The MNE-connectivity toolbox was employed to draw the figures for all the subjects. In Fig. 8, the figures of S1 to S4 are shown, in which each curve illustrates the average PLI strength of all epochs between each channel, and the selected range was 10–25 Hz. Only the strongest 12 connections were visualized, so the intensity of the displayed connections were approximately at the same level. It can be seen that all subjects have EEG-EMG couplings, and EEG channels CZ, C3, and C4 have the strongest connections to the muscles for the majority of subjects. This may be the reason why only adding C3 and C4 channels can considerably improve the recognition accuracy. In the figure of S1, apart from the EEG-EMG connections, the connections of CPZ with C4, CZ, C3, FZ are visible. For S3, both the connections of EEG-EMG and EEG-EEG are visualized. On the contrary, only EEG-EMG connections are visible in the figures of S2 and S4. This phenomenon was also found in the analysis of other subjects. Therefore, it is assumed that the subjects with comparable EEG-EMG connections and EEG-EEG connections will get greater benefits from the graph fusion method. For further investigation, the average Pearson coefficient matrices of all epochs for each subject were calculated. It was found that for the subjects with lower accuracy improvement, the Pearson coefficient of EEG-EMG was especially low. On the contrary, for the subjects with higher accuracy improvement, the values of the Pearson coefficient of both the EEG-EMG connections and EEG-EEG connections were relatively significant. Taking subjects 4 and 5 as examples, their Pearson coefficient matrices are visualized in Fig. 9.

The results of experiment II.C also suggest the essential difference of functional connectivity in the time and frequency domains. The average accuracies of the time-domain group (Pearson coefficient and mutual information) were higher than those of the frequency-domain group (coherence). Moreover, the Pearson coefficient and coherence are linear descriptions [30], while mutual information presents the coupling in a nonlinear way [31]. It seems that whether the connectivity is linear or nonlinear does not affect the performance significantly, but the domain of connectivity has an effect.

The aim of this paper is to find a connectivity that suitable for both of the connections. When computing the functional connectivity, the window length is 400ms, that is enough to include the segments of EEG and sEMG signals those have causation, as well as the synchronization of EEG-EEG signals. Therefore, this method can represent the real intention model of human's movement. However, the distance and interactions of EEG-EEG connections and EEG-sEMG connections are different. Using only one connectivity method to describe all the connections may not be completely justified. In the future, different connectivity approaches should be investigated for different edges.

E. The Future of Using Graphs to Fuse EEG and sEMG Signals

Multi-modal fusion is a promising direction in signal processing [12], and graph neural networks are also a novel research direction [23]. This paper is only a preliminary attempt to use graph neural networks to fuse EEG and sEMG signals, and there is much room for further improvement. First, only four topologies of fusion graphs were tested in this work, as the main objective was to study the effects of the number of EEG channels and the EMG-EMG connections. There likely exist other topologies that can provide better accuracy and robustness. Second, the node features of the fusion graph are segments of temporal signals, which retain the highest degree of intrinsic information but also may cause the problems of over-fitting and excessive computation. In the future, the use of the extracted features of EEG and sEMG as the node features should be investigated. Third, the Pearson coefficient is employed as the weights for all the edges, which may not be the best setting. Because of the objective differences between EEG and sEMG signals, employing customized connectivity for EEG-EMG and EEG-EEG edges may contribute to better performance. Finally, the improvement fluctuates from subject to subject, which indicates the challenge of subject dependency of this method. This is due to the EEG signals of some subjects are naturally weak, and cannot provide valuable information. Next, this problem may be studied by using more proper connectivity or modifying the neural network or preprocessing the EEG signals before fusing to reduce variance. In addition, there are many approaches by which to manifest functional connectivity, such as the phase-locking value (PLV), transfer entropy, partial directed coherence (PDC), etc. It is therefore worth studying different connectivity methods to improve the performance of fusion graphs.

V. Conclusion

In this work, a novel end-to-end multi-modal fusion approach of EEG and sEMG signals using the GCN was proposed. In terms of this fusion graph, topologies, standardization methods, and functional connectivity were investigated. The 2EnMe topology with min-max standardization for node features and the Pearson coefficient as the weights of edges was found to be the best model. It achieved average accuracies of eight subjects of 93.86% and 91.23% at the fatigue levels of 0% and 30%, respectively. The accuracy decrease ratio (ADR) was employed to quantify the robustness. The ADR of 2EnMe-Pearson was 2.80%, which was found to be considerably better than those of the CNN with parallel fusion (7.87%) and the CNN with single-modality EMG (11.15%). Based on the experimental results, it can be concluded that the use of graphs to fuse EEG and sEMG signals can improve the robustness to resist abnormal data or fatigue data, and it can achieve higher accuracy as compared with the single-modality method. The proposed graph fusion method has the potential to

improve the reliability of active rehabilitation for stroke patients. In the future, its topological structure and connections can be studied to achieve better performance.

ACKNOWLEDGMENT

The authors thank the participants and all those who provided help and advice in the experiment.

REFERENCES

[1] D. Lynch, M. Ferraro, J. Krol, C. M. Trudell, P. Christos, and B. T. Volpe, "Continuous passive motion improves shoulder joint integrity following stroke," *Clinical Rehabilitation*, vol. 19, no. 6, p. 594, 2005.

[2] Miao Q, Zhang M M, Cao J H, et al. Reviewing high-level control techniques on robot-assisted upper-limb rehabilitation[J]. *Advanced Robotics*, 2018, 32(24): 1253-1268.

[3] K. K. Ang and C. Guan, "Brain-Computer Interface in Stroke Rehabilitation," *J. Comput. Sci. Eng.*, vol. 7, no. 2, pp. 139–146, 2013.

[4] M. Mahmood, S. Kwon, H. Kim, Y. S. Kim, P. Siriaraya, J. Choi, "Wireless Soft Scalp Electronics and Virtual Reality System for Motor Imagery-Based Brain-Machine Interfaces," *Adv Sci (Weinh)*, p. e2101129, Jul. 2021, doi: 10.1002/advs.202101129.

[5] M. S. Al-Quraishi, I. Elamvazuthi, T. B. Tang, M. Al-Qurishi, S. Parasuraman, and A. Borboni, "Multimodal Fusion Approach Based on EEG and EMG Signals for Lower Limb Movement Recognition," *IEEE Sensors Journal*, vol. 21, no. 24, pp. 27640-27650, 2021, doi: 10.1109/jsen.2021.3119074.

[6] D. Leonardis, M. Barsotti, C. Loconsole, M. Solazzi, M. Troncossi, C. Mazzotti, "An EMG-Controlled Robotic Hand Exoskeleton for Bilateral Rehabilitation," *IEEE Transactions on Haptics*, vol. 8, no. 2, pp. 140-151, 2015.

[7] S. Wist, J. Clivaz, and M. Sattelmayer, "Muscle strengthening for hemiparesis after stroke: A meta-analysis," *Ann Phys Rehabil Med*, vol. 59, no. 2, pp. 114-24, Apr. 2016.

[8] R. M. Enoka and J. Duchateau, "Muscle fatigue: what, why and how it influences muscle function," *J Physiol*, vol. 586, no. 1, pp. 11-23, Jan. 2008, doi: 10.1113/jphysiol.2007.139477.

[9] R. Leeb, H. Sagha, R. Chavarriaga, and R. Millan Jdel, "A hybrid brain-computer interface based on the fusion of electroencephalographic and electromyographic activities," *J Neural Eng*, vol. 8, no. 2, p. 025011, Apr. 2011, doi: 10.1088/1741-2560/8/2/025011.

[10] X. Li, O. W. Samuel, X. Zhang, H. Wang, P. Fang, and G. Li, "A motion-classification strategy based on sEMG-EEG signal combination for upper-limb amputees," *J Neuroeng Rehabil*, vol. 14, no. 1, p. 2, Jan. 2017, doi: 10.1186/s12984-016-0212-z.

[11] A. Chowdhury, H. Raza, Y. K. Meena, A. Dutta, and G. Prasad, "An EEG-EMG correlation-based brain-computer interface for hand orthosis supported neuro-rehabilitation," *J Neurosci Methods*, vol. 312, pp. 1-11, Jan. 2019, doi: 10.1016/j.jneumeth.2018.11.010.

[12] T. Baltrusaitis, C. Ahuja, and L. P. Morency, "Multimodal Machine Learning: A Survey and Taxonomy," *IEEE Trans Pattern Anal Mach Intell*, vol. 41, no. 2, pp. 423-443, Feb. 2019, doi: 10.1109/TPAMI.2018.2798607.

[13] Z. Tang, H. Yu, C. Lu, P. Liu, and X. Jin, "Single-trial classification of different movements on one arm based on ERD/ERS and corticomuscular coherence," *IEEE Access*, vol. 7, pp. 128185–128197, 2019, doi: 10.1109/ACCESS.2019.2940034.

[14] Z. Jiao, X. Gao, Y. Wang, J. Li, and H. Xu, "Deep convolutional neural networks for mental load classification based on EEG data," *Pattern Recognition*, vol. 76, pp. 582–595, 2018.

[15] D. Zhang, K. Ch en, D. Jian, and L. Yao, "Motor Imagery Classification via Temporal Attention Cues of Graph Embedded EEG Signals," *IEEE J Biomed Health Inform*, vol. 24, no. 9, pp. 2570-2579, Sep. 2020, doi: 10.1109/JBHI.2020.2967128.

[16] T. Song, W. Zheng, P. Song, and Z. Cui, "EEG Emotion Recognition Using Dynamical Graph Convolutional Neural Networks," *IEEE Transactions on Affective Computing*, vol. 11, no. 3, pp. 532-541, 2020, doi: 10.1109/taffc.2018.2817622.

[17] V. Siemionow, V. Sahgal, and G. H. Yue, "Single-Trial EEG-EMG coherence analysis reveals muscle fatigue-related progressive alterations in corticomuscular coupling," *IEEE Trans Neural Syst Rehabil Eng*, vol. 18, no. 2, pp. 97-106, Apr. 2010, doi: 10.1109/TNSRE.2010.2047173.

[18] F. Fahimi, Z. Zhang, W. B. Goh, T. S. Lee, K. K. Ang, and C. Guan, "Inter-subject transfer learning with an end-to-end deep convolutional neural network for EEG-based BCI," *J Neural Eng*, vol. 16, no. 2, p. 026007, Apr. 2019, doi: 10.1088/1741-2552/aaf3f6.

[19] Y. Hou, L. Zhou, S. Jia, and X. Lun, "A novel approach of decoding EEG four-class motor imagery tasks via scout ESI and CNN," *J Neural Eng*, vol. 17, no. 1, p. 016048, Feb. 2020, doi: 10.1088/1741-2552/ab4af6.

[20] F. P. Such, S. Sah, M. A. Dominguez, S. Pillai, Z. Chao, A. Michael, "Robust Spatial Filtering with Graph Convolutional Neural Networks," *IEEE Journal of Selected Topics in Signal Processing*, vol. PP, no. 6, pp. 1-1, 2017.

[21] Y. Li, X. R. Zhang, B. Zhang, M. Y. Lei, W. G. Cui, and Y. Z. Guo, "A Channel-Projection Mixed-Scale Convolutional Neural Network for Motor Imagery EEG Decoding," IEEE Trans Neural Syst Rehabil Eng, vol. 27, no. 6, pp. 1170-1180, Jun. 2019, doi: 10.1109/TNSRE.2019.2915621.

[22] Q. Zhang, J. Zhou, and B. Zhang, "Graph Based Multichannel Feature Fusion for Wrist Pulse Diagnosis," *IEEE J Biomed Health Inform*, vol. 25, no. 10, pp. 3732-3743, Oct 2021, doi: 10.1109/JBHI.2020.3045274.

[23] Z. Wu, S. Pan, F. Chen, G. Long, C. Zhang, and P. S. Yu, "A Comprehensive Survey on Graph Neural Networks," *IEEE Trans Neural Netw Learn Syst*, vol. 32, no. 1, pp. 4-24, Jan. 2021, doi: 10.1109/TNNLS.2020.2978386.

[24] W. L. Hamilton, R. Ying, and J. Leskovec, "Inductive representation learning on large graphs," presented at the Proceedings of the *31st International Conference on Neural Information Processing Systems*, Long Beach, California, USA, 2017.

[25] X. Xi et al., "Enhanced EEG–EMG coherence analysis based on hand movements," *Biomedical Signal Processing and Control*, vol. 56, 2020, doi: 10.1016/j.bspc.2019.101727.

[26] Björn et al., "Criterion validation of surface EMG variables as fatigue indicators using peak torque: a study of repetitive maximum isokinetic knee extensions," *Journal of Electromyography & Kinesiology*, 2000.

[27] N. A. Dimitrova and G. V. Dimitrov, "Interpretation of EMG changes with fatigue: facts, pitfalls, and fallacies," *Journal of Electromyography and Kinesiology*, vol. 13, no. 1, pp. 13-36, 2003, doi: 10.1016/s1050-6411(02)00083-4.

[28] A. R. V. de, J. C. do Carmo, and O. N. F. Assis de, "Weighted-Cumulated S-EMG Muscle Fatigue Estimator," *IEEE J Biomed Health Inform*, vol. 22, no. 6, pp. 1854-1862, Nov 2018, doi: 10.1109/JBHI.2017.2783849.

[29] G. Pfurtscheller and F. Silva, "Event-related EEG/MEG synchronization and desynchronization," *Clinical Neurophysiology*, vol. 110, no. 11, pp. 1842-1857, 1999.

[30] P. Mathur and V. K. Chakka, "Graph Signal Processing Based Cross-Subject Mental Task Classification Using Multi-Channel EEG Signals," *IEEE Sensors Journal*, vol. 22, no. 8, pp. 7971-7978, 2022, doi: 10.1109/jsen.2022.3156152.

[31] J. Gao et al., "Brain Fingerprinting and Lie Detection: A Study of Dynamic Functional Connectivity Patterns of Deception Using EEG Phase Synchrony Analysis," *IEEE J Biomed Health Inform*, vol. 26, no. 2, pp. 600-613, Feb. 2022, doi: 10.1109/JBHI.2021.3095415.

[32] B. Kim, L. Kim, Y.-H. Kim, and S. K. Yoo, "Cross-association analysis of EEG and EMG signals according to movement intention state," *Cognitive Systems Research*, vol. 44, pp. 1-9, 2017, doi: 10.1016/j.cogsys.2017.02.001.

[33] C. L. Witham, C. N. Riddle, M. R. Baker, and S. N. Baker, "Contributions of descending and ascending pathways to corticomuscular coherence in humans," *J Physiol*, vol. 589, no. Pt 15, pp. 3789-800, Aug. 2011, doi: 10.1113/jphysiol.2011.211045.

[34] T. N. Kipf and M. Welling, "Semi-Supervised Classification with Graph Convolutional Networks,", arXiv:1609.02907, 2016.

[35] Q. Li, Z. Han, and X. M. Wu, "Deeper insights into graph convolutional networks for semi-supervised learning," in *Proc. AAAI Conf.Artif. Intell*., 2018, pp. 3538–3545.

[36] T. Zhang, X. Wang, X. Xu, and C. L. P. Chen, "GCB-Net: Graph Convolutional Broad Network and Its Application in Emotion Recognition," *IEEE Transactions on Affective Computing*, vol. 13, no. 1, pp. 379-388, 2022.

[37] M. Vinck, R. Oostenveld, M. van Wingerden, F. Battaglia, and C. M. Pennartz, "An improved index of phase-synchronization for electrophysiological data in the presence of volume-conduction, noise and sample-size bias," *Neuroimage*, vol. 55, no. 4, pp. 1548-65, Apr. 2011.

[38] J. Tryon, E. Friedman and A. L. Trejos, "Performance Evaluation of EEG/EMG Fusion Methods for Motion Classification," *2019 IEEE 16th*

International Conference on Rehabilitation Robotics (ICORR), 2019, pp. 971-976, doi: 10.1109/ICORR.2019.8779465.

Shiqi Yang received the B.S. degree in Automobile Engineering from Hefei University of Technology, Hefei, China, in 2020. He is currently pursuing the M.Phil degree in Mechanical Engineering in the School of Mechanical Engineering, Xi'an Jiaotong University, Xi'an, China. His research interests include rehabilitation robots, signal processing and brain-computer interface (BCI).

Min Li is an Associate Professor at the School of Mechanical Engineering, Xi'an Jiaotong University, China. She received her B.Sc. degree in Mechanical Engineering and her M.Sc. degree in Agricultural Mechanization Engineering from Northwest A&F University, China, in 2007 and 2010, respectively. She was awarded the Ph.D. degree in Robotics at King's College London, UK, in 2014. From 2015 to 2017, she was a Lecturer with Xi'an Jiaotong University. Her research interests include haptic feedback for robots, soft robots and rehabilitation robots.

Jiale Wang received the B.S. degree in agricultural mechanization and automation from Henan University of Science and Technology, Henan, China, in 2020. He is currently pursuing the M.S degree in Mechanical Engineering with the School of Mechanical Engineering, Xi'an Jiaotong University, Xi'an, China. His research interests include rehabilitation robots and sEMG signal processing.